Study of baryon form factor at BESIII

Bingxin Zhang

On behalf of BESIII collaboration

Dec. 16-18 2019

BINP-IHEP Seminar @BINP SB RAS

Outline

- **Introduction**
- **$e^+e^- \to p\bar{p}$ and $n\bar{n}$ analysis**
- **$e^+e^- \to \Lambda\bar{\Lambda}$ and $\Lambda_c^+\bar{\Lambda}_c^-$analysis**
- **Summary & Outlook**

Introduction(I)

Electromagnetic Form Factors of the Nucleon

- **Electromagnetic form factors** characterize the internal structure and dynamics of nucleon.

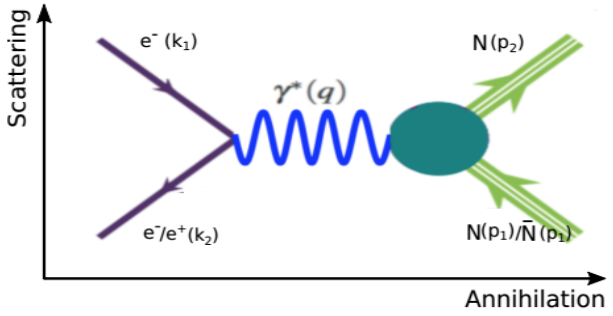

- Scattering amplitude in Born approximation:

$$\mathcal{M} = \frac{1}{q^2}\,[e\,\bar{u}(k_2)\gamma_\mu u(k_1)]\,\underbrace{[e\,\bar{U}(p_2)\Gamma^\mu(p_1,p_2)U(p_1)]}_{\text{Nucleon EM 4-current: } J_N^\mu}$$

- The electromagnetic vertex of nucleon:

$$\Gamma^\mu = \gamma^\mu F_1^N(q^2) + \frac{i\sigma^\mu_\nu q^\nu}{2M} F_2^N(q^2)$$

$F_1^N(q^2)$: **Dirac FF.**
$F_2^N(q^2)$: **Pauli FF.**

- Combination of Pauli and Dirac FFs leads to the so called **Sachs FFs**:

$$G_E = F_1(q^2) + (q^2/4M^2)F_2(q^2) \qquad G_M = F_1(q^2) + F_2(q^2)$$

How experimentally the Form Factors are determined?

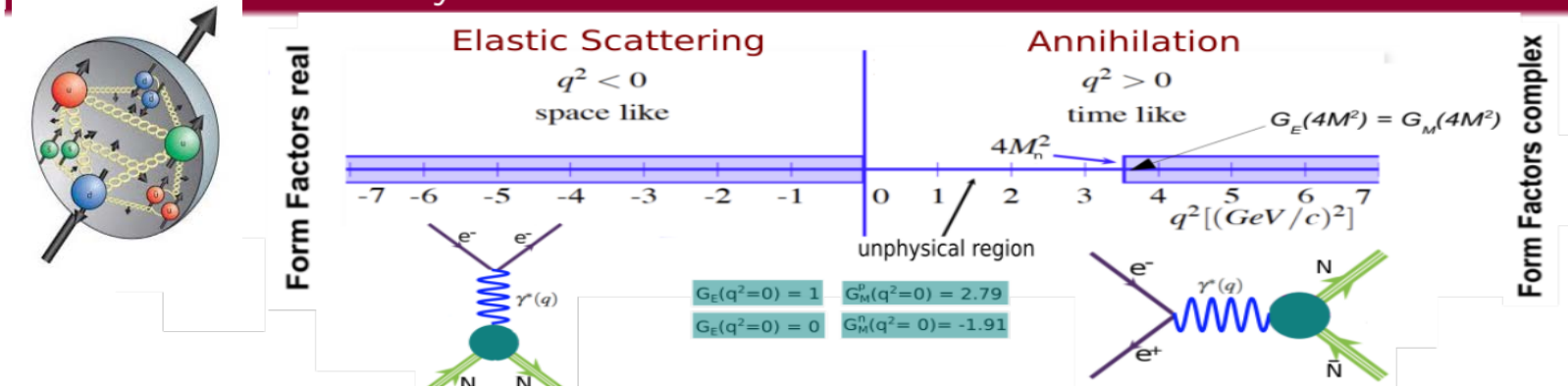

- Time-like FF's are complex, $G_E = |G_E|e^{i\Phi_E}$, $G_M = |G_M|e^{i\Phi_M}$ Relative phase: $\Delta\Phi(q^2) = \Phi_E - \Phi_M$
- A non-zero phase has polarization effect on the Baryons, even for unpolarized initial state: $P_y \propto \sin\Delta\Phi$

Introduction(II)

Hyperons – key to the strong interaction

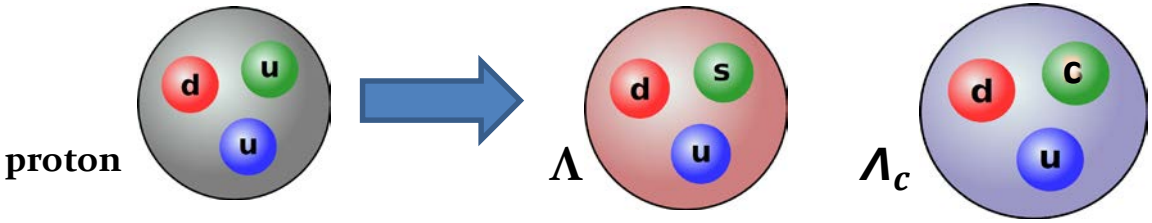

- Systems with strangeness
  - Scale: $m_s \approx 100$ MeV ~ $\Lambda_{QCD} \approx 200$ MeV: Relevant degrees of freedom?
  - **Probes QCD in the confinement domain.**
- Systems with charm
  - Scale: $m_c \approx 1300$ MeV: Quarks and gluons more relevant.
  - **Probes QCD just below pQCD.**
- The angular distribution of daughter baryon from Hyperon weak decay is: $\frac{d\sigma}{d\Omega} \propto 1 + \alpha_\Lambda \boldsymbol{P_y} \cdot \hat{\boldsymbol{q}}$
  - α_Λ: asymmetry parameter
  - $\hat{q}$: unit vector along the daughter baryon in hyperon rest frame

Polarization experimentally accessible by the weak, parity violating decay

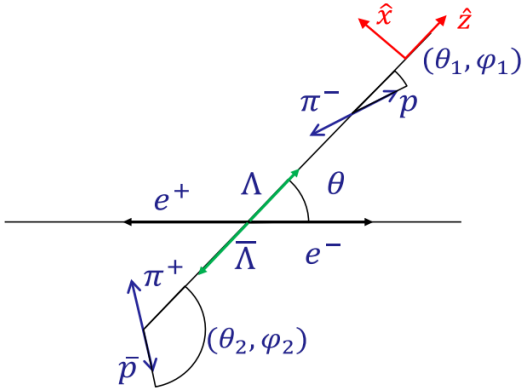

Example: Angular distribution of $\Lambda \rightarrow p\pi^-$

$I(\cos\theta_p) = N(1+\alpha_\Lambda P_\Lambda \cos\theta_p)$

$P_\Lambda = P_\Lambda(\cos\theta_\Lambda)$: polarisation (production)

α_Λ : asymmetry parameter (decay)

BESIII data samples

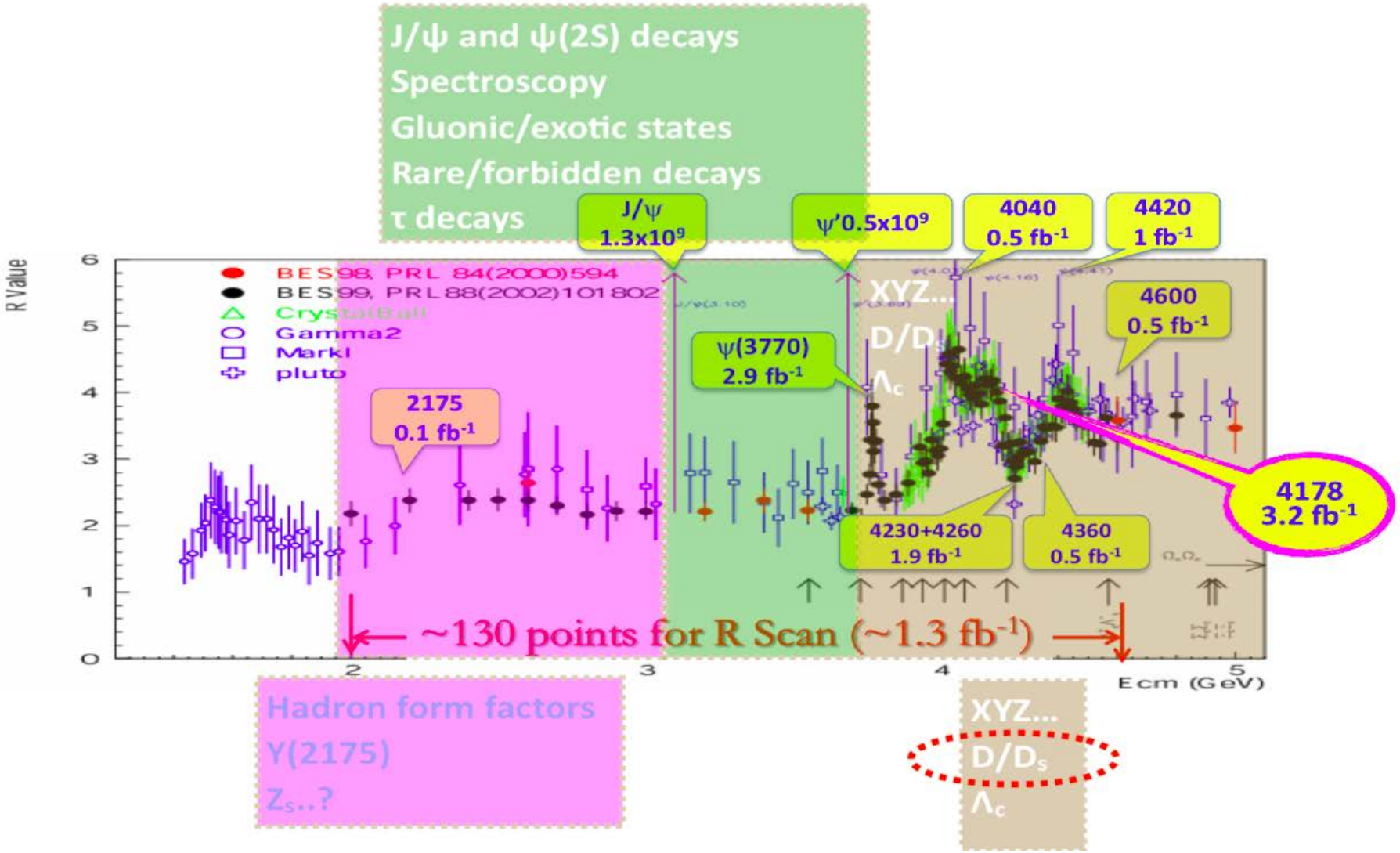

Measurement of nucleon form factor by studying $e^+e^- \rightarrow p\bar{p}$

Selection Criteria

1. Two charged tracks from the vertex
2. $|\cos\theta|<0.93$ (0.80 for $\sqrt{s}>2.4$GeV)
3. PID (tof & dE/dx)
4. $\theta_{p\bar{p}}<178^0(179^0)$
5. $|p_{mea}-p_{exp}|<5\sigma_p$

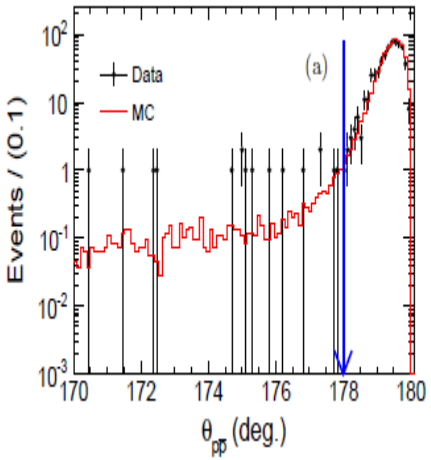

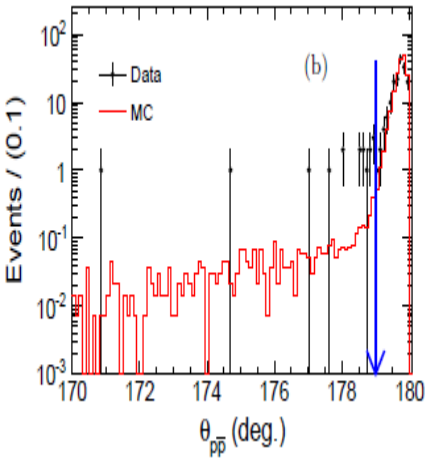

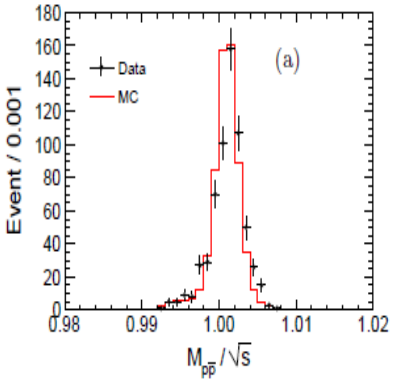

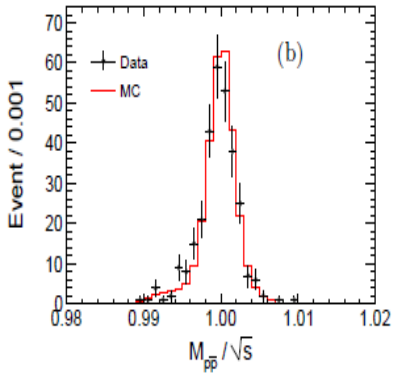

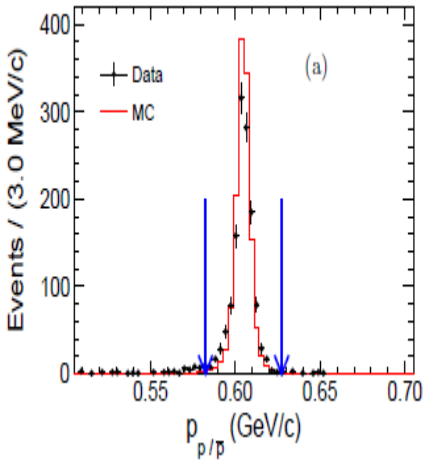

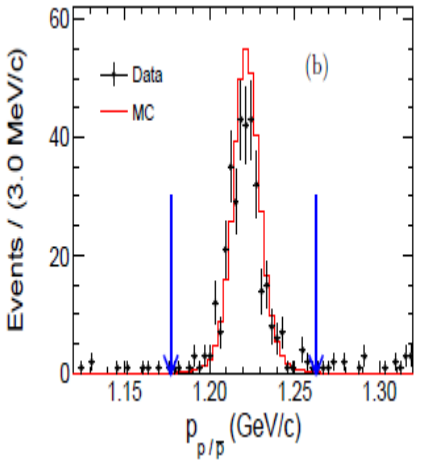

Background analysis

	E_{cm} = 2.2324			($\mathfrak{L}$=2.634 pb^{-1})
Bkg	N_{gen}^{MC}	N_{sur}^{MC}	$\sigma(nb)$	$N_{uplimit}^{data}$(90% CL)
e^+e^-	9.6×10^6	0	1434.01	< 0.96
$\mu^+\mu^-$	7.0×10^5	0	17.41	< 0.16
$\gamma\gamma$	1.9×10^6	0	70.44	< 0.24
$\pi^+\pi^-$	1.0×10^5	0	0.173	< 0.01
K^+K^-	1.0×10^5	0	0.138	< 0.008
$p\bar{p}\pi^0$	1.0×10^5	0	< 0.1	< 0.006
$p\bar{p}\pi^0\pi^0$	1.0×10^5	0	< 0.1	< 0.006
$\Lambda\bar{\Lambda}$	1.0×10^5	0	0.4	< 0.02

	E_{cm} = 3.08			($\mathfrak{L}$=30.73 pb^{-1})
Bkg	N_{gen}^{MC}	N_{sur}^{MC}	$\sigma(nb)$	$N_{uplimit}^{data}$(90% CL)
e^+e^-	3.99×10^7	1	756.86	< 2.54
$\mu^+\mu^-$	1.50×10^6	0	8.45	< 0.42
$\gamma\gamma$	4.5×10^6	0	37.05	< 0.62
$\pi^+\pi^-$	1.0×10^5	0	< 0.111	< 0.02
K^+K^-	1.0×10^5	0	0.0933	< 0.02
$p\bar{p}\pi^0$	1.0×10^5	0	< 0.1	< 0.07
$p\bar{p}\pi^0\pi^0$	1.0×10^5	0	< 0.1	< 0.07
$\Lambda^0\bar{\Lambda}^0$	1.0×10^5	0	0.002	0.001

	E_{cm} = 3.65			($\mathfrak{L}$=48.823 pb^{-1})
Bkg	N_{gen}^{MC}	N_{sur}^{MC}	$\sigma(nb)$	N_{mix}^{data} (90% CL)
e^+e^-	4.44×10^7	1	537.46	< 2.58
$\mu^+\mu^-$	1.5×10^6	0	6.50	< 0.52
$\gamma\gamma$	5.5×10^6	0	26.33	< 0.57
$\pi^+\pi^-$	1.0×10^5	0	0.044	< 0.01
K^+K^-	1.0×10^5	0	0.0400	< 0.01
$p\bar{p}\pi^0$	1.0×10^5	0	< 0.1	< 0.1
$p\bar{p}\pi^0\pi^0$	1.0×10^5	0	< 0.1	< 0.1
$\Lambda^0\bar{\Lambda}^0$	1.0×10^5	0	0.002	< 0.002
$\tau\tau$	1.0×10^6	0	2.0	< 0.1

E_{cm} (GeV)	N_{pro}^{data}	N_{sur}^{data}
2.40	9412203	0
3.40	13191714	0

Separated beam data

Background events are almost negligible

Result of analysis

Energy scan method

$\sqrt{s}$ (MeV)	N_{obs}	N_{bkg}	ε' (%)	L (pb^{-1})	σ_{Born} (pb)	$\lvert G\rvert$ ($\times 10^{-2}$)
2232.4	614 ± 25	1	66.00	2.63	$353.0 \pm 14.3 \pm 15.5$	$16.10 \pm 0.32 \pm 0.35$
2400.0	297 ± 17	1	65.79	3.42	$132.7 \pm 7.7 \pm 8.1$	$10.07 \pm 0.29 \pm 0.31$
2800.0	53 ± 7	1	65.08	3.75	$21.3 \pm 3.0 \pm 2.8$	$4.45 \pm 0.31 \pm 0.29$
3050.0	91 ± 10	2	59.11	14.90	$10.1 \pm 1.1 \pm 0.6$	$3.29 \pm 0.17 \pm 0.09$
3060.0	78 ± 9	2	59.21	15.06	$8.5 \pm 1.0 \pm 0.6$	$3.03 \pm 0.17 \pm 0.10$
3080.0	162 ± 13	1	58.97	30.73	$8.9 \pm 0.7 \pm 0.5$	$3.11 \pm 0.12 \pm 0.08$
3400.0	2 ± 1	0	63.34	1.73	$1.8 \pm 1.3 \pm 0.4$	$1.54 \pm 0.55 \pm 0.18$
3500.0	5 ± 2	0	63.70	3.61	$2.2 \pm 1.0 \pm 0.6$	$1.73 \pm 0.39 \pm 0.22$
3550.7	24 ± 5	1	62.23	18.15	$2.0 \pm 0.4 \pm 0.6$	$1.67 \pm 0.17 \pm 0.23$
3600.2	14 ± 4	1	62.24	9.55	$2.2 \pm 0.6 \pm 0.9$	$1.78 \pm 0.25 \pm 0.35$
3650.0	36 ± 6	4	61.20	48.82	$1.1 \pm 0.2 \pm 0.1$	$1.26 \pm 0.11 \pm 0.07$
3671.0	6 ± 2	0	51.17	4.59	$2.2 \pm 0.9 \pm 0.8$	$1.84 \pm 0.37 \pm 0.33$

$$\sigma_{Born} = \frac{N_{obs} - N_{bkg}}{\mathcal{L} \cdot \varepsilon \cdot (1+\delta)}$$

$$|G| = \sqrt{\frac{\sigma_{Born}}{86.83 \cdot \frac{\beta}{s}\left(1 + \frac{2m_p^2}{s}\right)}}$$

Comparison with other Experiment

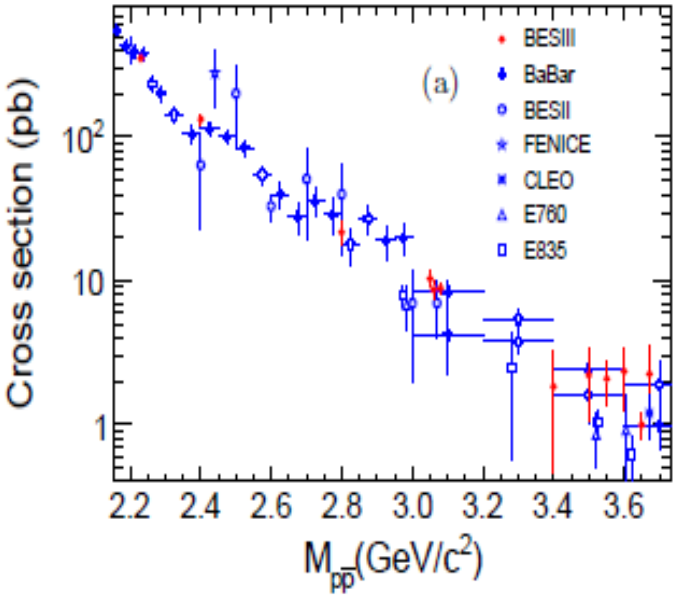

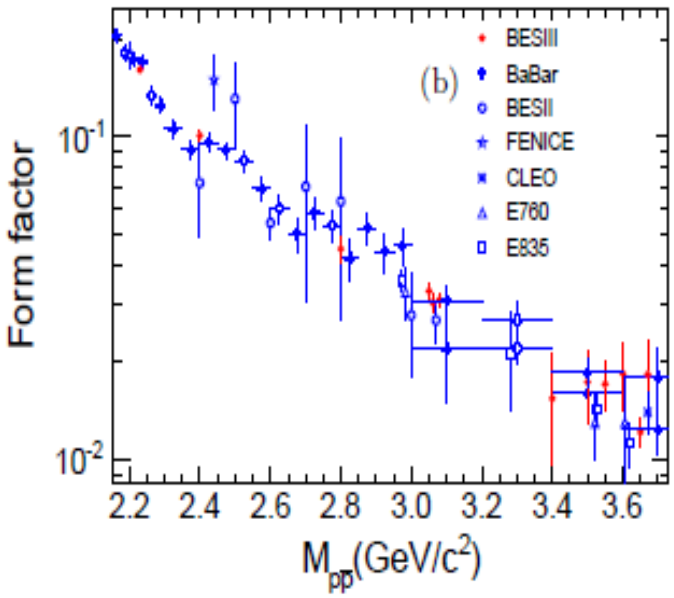

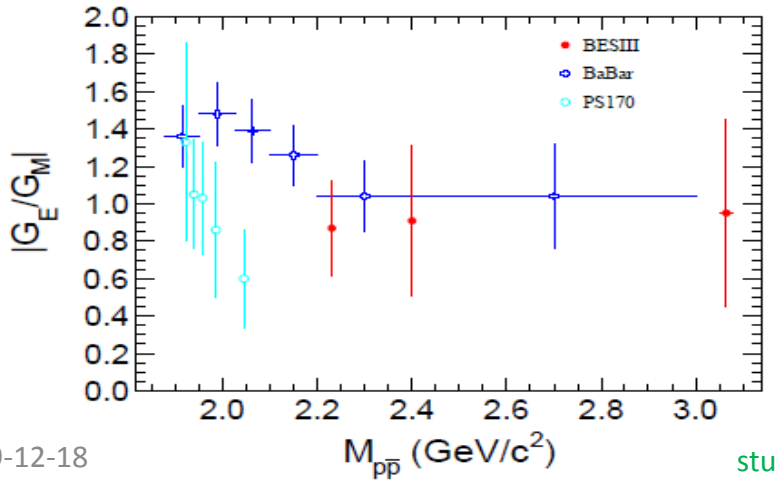

1. $|G_E|$ and $|G_M|$ extracted individually
2. Precision between 11% and 28%
3. Consistent with previous one at same q-range 12 c.m. energy

Phys. Rev. D91, 112004 (2015)

ISR-Tagged Analysis for Proton

ISR method

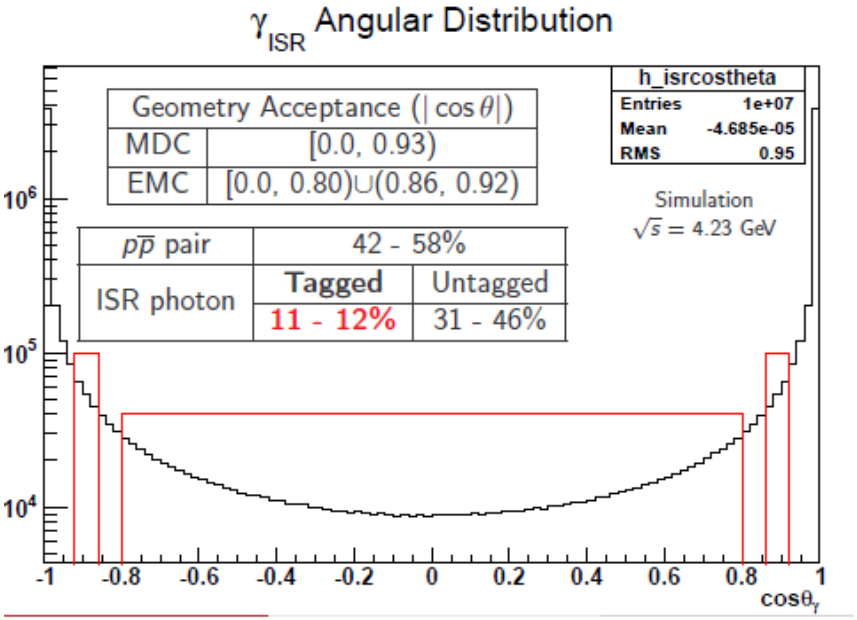

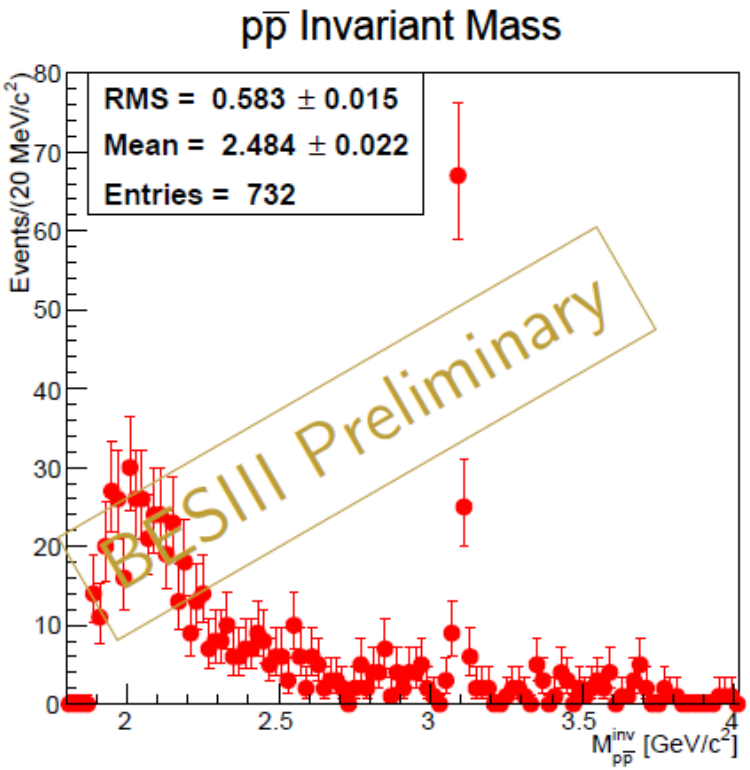

- 7 data samples ($\geq$ 3.773 GeV)
- Total luminosity 7.4 fb^{-1}
- Event selction:
  - Two charged tracks from vertex
  - One high energy shower in EMC
  - Kinematic constraints applied
- Background evaluation

Data at the energy 4.23 GeV

$p\bar{p}$ invariant mass spectrum from threshold

Results from ISR-Tagged Analysis

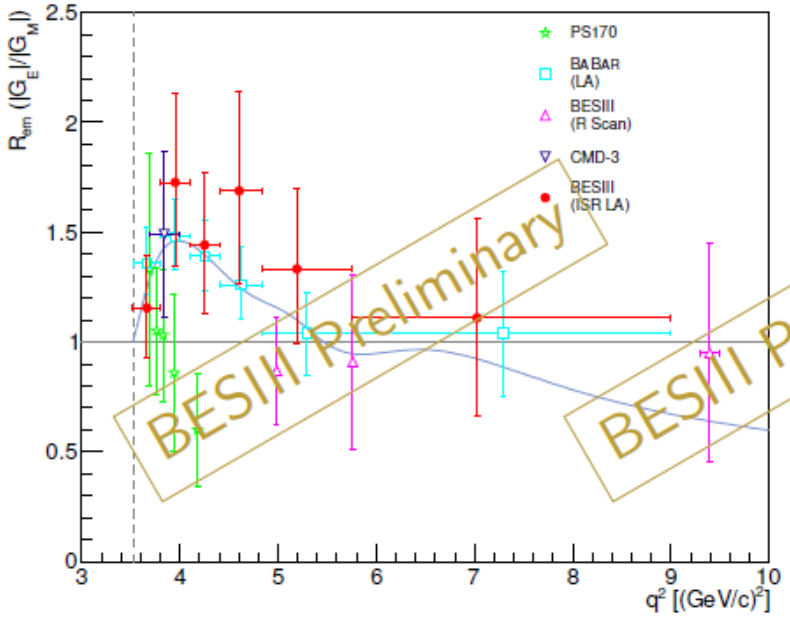

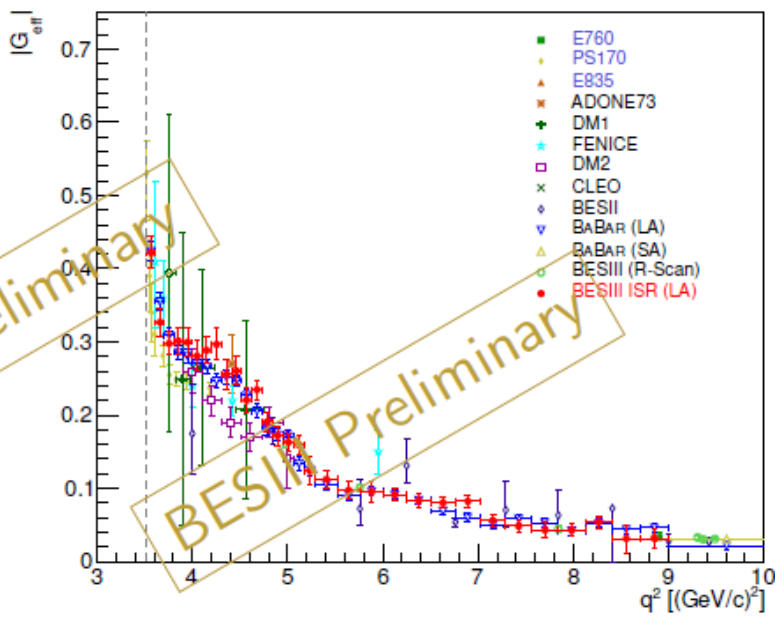

- Background subtraction and efficiency dividing
- Combine the seven data samples
- The proton FFs extracted between th. – 3.0 GeV
- Systematic uncertainty included

	$\frac{\delta R_{em}}{R_{em}}$	$\frac{\delta G_{eff}}{G_{eff}}$
stat.	16% - 34%	5% - 32%
syst.	5% - 22%	2% - 30%

LA: **L**arge polar **A**ngle of ISR photon
SA: **S**mall polar **A**ngle of ISR photon

Measurement of nucleon form factor by studying $e^+e^- \rightarrow n\bar{n}$

Neutron Form Factors in the Space-and Time-Like Region

- **The electric and magnetic FFs had been measured in the SL region while not in the TL region.**

Space-Like region

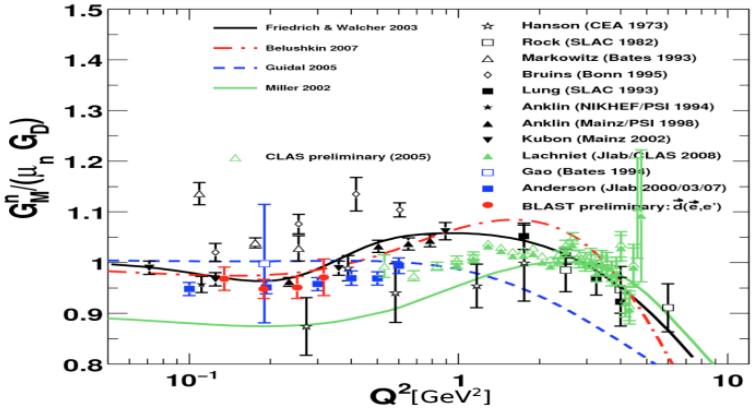

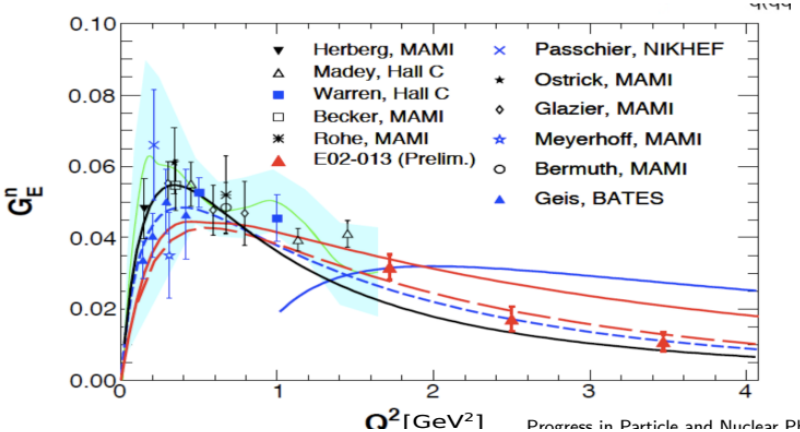

Progress in Particle and Nuclear Physics 59 (2007) 694-764

Time-Like region

No results for the neutron FFs (G_E^n and G_M^n).

Analysis Strategy

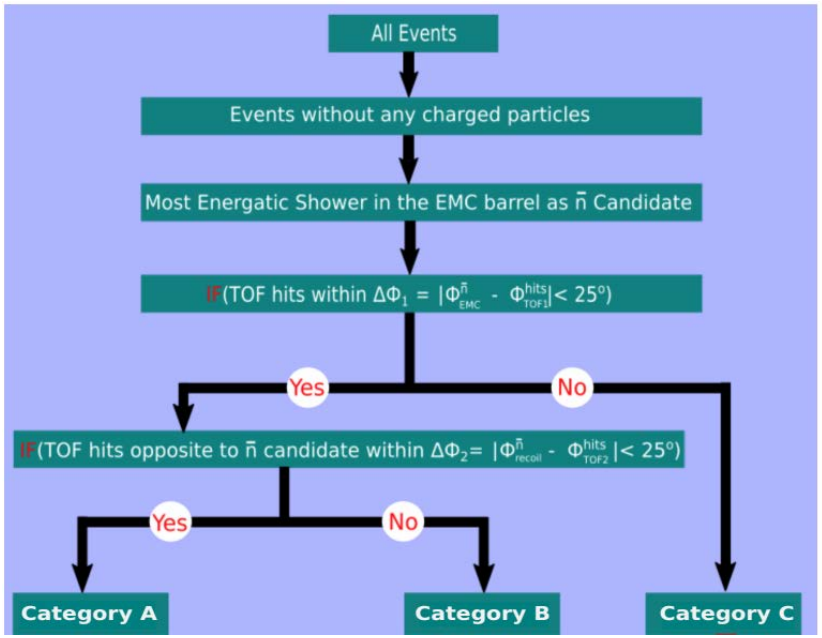

Category A

Selection	Value	Expression
$N_{charged}$	0	number of charged tracks without constraint on the vertex
$E_{\bar{n}}$	[0.5, 2.0] GeV	energy deposition of antineutron candidate (EMC1)
N^{50}_{HIT}	[30, 140]	number of hits in 50^o cone around antineutron
$\cos\theta$	[-0.7, 0.7]	cosine of polar angle of antineutron
$\Delta\phi_{(TOF1,EMC1)}$	$[-3\phi_c, 3\phi_c]$ rad.	azimuthal constraints on antineutron
$\theta_{(TOF1,EMC1)}$	[-0.5, 0.5] rad.	crossing angle between EMC1 and TOF1 for antineutron
$\Delta\phi_{(TOF2,EMC1)}$	$[-6\phi_c, 6\phi_c]$ rad.	azimuthal constraints on neutron
ΔT_n	[-4, 4] ns	the measured time difference from the expected for neutron
E_n	(, 0.7) [0.06, 0.7] GeV	energy deposition in EMC2 of neutron
$\theta_{TOF2',EMC1}$	3.0 [2.98] rad.	crossing angle between TOF2' of neutron and EMC1 of antineutron
ΔT	[-4.0, 4.0] ns	time difference between TOF2' of neutron and TOF1 of antineutron
$\theta_{EMC2,EMC1}$	[3.0,] rad.	crossing angle between EMC2 of neutron and EMC1 of antineutron

Category B

Selection	Value	Expression
$N_{charged}$	0	number of charged tracks without constraint on the vertex
$E_{\bar{n}}$	[0.5, 2.0] GeV	energy deposition of antineutron candidate (EMC1)
$\cos\theta$	[-0.7, 0.7]	cosine of polar angle of antineutron
$\Delta\phi_{(TOF1,EMC1)}$	$[-3\phi_c, 3\phi_c]$ rad.	azimuthal constraints on antineutron
$\theta_{(TOF1,EMC1)}$	[-0.5, 0.5] rad.	crossing angle between EMC1 and TOF1 for antineutron
$\lvert\Delta T_\gamma\rvert$	> 0.5 ns	the measured time difference in hypothesis of photon
BDT	> 0.1	the BDT discriminator with seven $\bar{n}$ related variables
E_n	[0.04/0.06, 0.6] GeV	energy deposition of neutron candidate ($\sqrt{s} \leq$ / $>$ 2.3094 GeV
ll_{muc}	< 6	last layer with hits in the MUC
$\sphericalangle^n_{\bar{n}}$	$> 150^o$	opening angle between the n and $\bar{n}$ candidate in the calorimeter

Category C

Selection	Value	Expression
$N_{charged}$	== 0	number of charged tracks without constrain on the vertex
$E_{\bar{n}}$	[0.5, 2.0] GeV	energy deposition of antineutron candidate in the calorimeter
2 $moment_{\bar{n}}$	>20 cm^2	second moment of antineutron candidate, 2 $moment_{\bar{n}} = \sum_i E_i r_i^2 / E_i$
N^{50}_{HIT}	[35, 100]	number of hits in 50^o cone around the $\bar{n}$ candidate
E_n	[0.04/0.06, 0.6] GeV	energy deposition of neutron candidate ($\sqrt{s} \leq$ / $>$ 2.3094 GeV
E_{extra}	$<$0.15 GeV	$E_{extra} = E_{total} - E^{50^o\,cone}_{\bar{n}} - E^{20^o\,cone}_{n}$
ll_{muc}	< 6	last layer with hits in the MUC
$\sphericalangle^n_{\bar{n}}$	$> 150^o$	opening angle between the n and $\bar{n}$ candidate in the calorimeter

Extraction of Signal Yield

- **The signal yields in the 3 categories are extracted by the fit where the variables used for the fit:**

Category A: $(\mathrm{EMC+TOF})_{\bar{n}}+(\mathrm{TOF})_n$

Category B: $(\mathrm{EMC+TOF})_{\bar{n}}+(\mathrm{EMC})_n$

Category C: $(\mathrm{EMC})_{\bar{n}}+(\mathrm{EMC})_n$

$$\Delta T_n \equiv T_{TOF2} - T_0^n - T_n$$

$$T_n = \frac{L}{\beta C}, \beta = \frac{\sqrt{E_{cm}^2 - m^2}}{E_{cm}}$$

$$\theta_{n,\bar{n}} \equiv \arccos\left(\frac{V_{EMC1} \cdot V_{EMC2}}{|V_{EMC1}||V_{EMC2}|}\right)$$

Category A

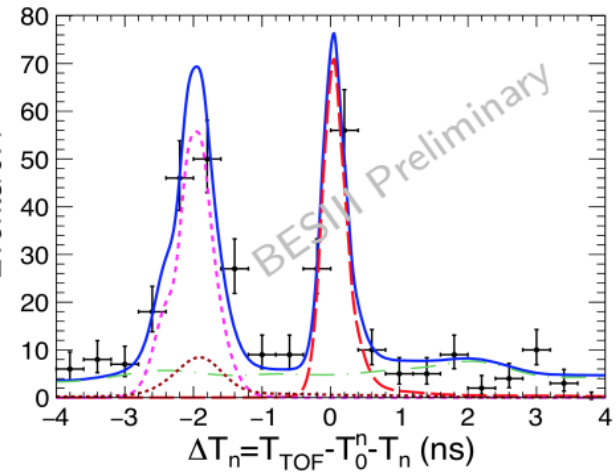

- Signal PDF: MC shape.
- Background PDF: data.

Category B

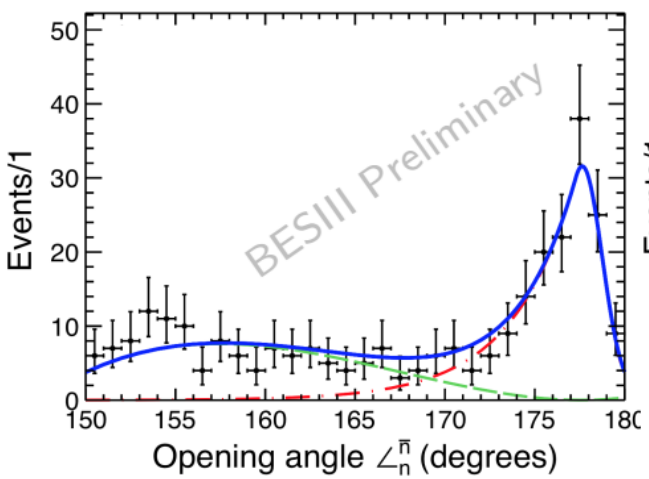

- Signal PDF: Crystal-ball function.
- Background PDF: three-order polynomial function.

Category C

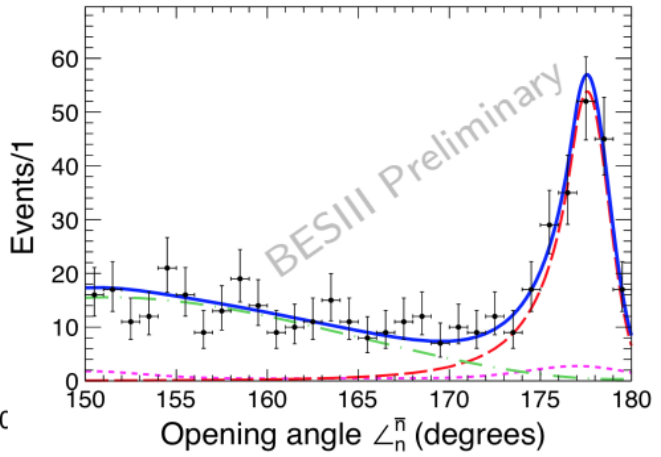

- Signal PDF: Crystal-ball function.
- Background PDF: Chebychev polynomial function of third order.

Cross section & FF calculation

Born Cross Section and Effective Form Factors

- Experimentally, the Born cross section of the $e^+e^- \to n\bar{n}$ process is determined via:

$$\sigma_{Born} = \frac{N_{data}}{\epsilon_{n\bar{n}}^{MC} \times \mathcal{C}_{dm} \times \mathcal{C}_{trg} \times (1+\delta) \times \mathcal{L}_{Int}}$$

N_{data}: Number of selected $n\bar{n}$ data events, $\mathcal{C}_{dm}$: data/MC efficiency correction, $\mathcal{C}_{trg}$: trigger efficiency correction.

$1+\delta$: Radiative correction and vacuum polarisation $(1+\delta)$, $\epsilon_{n\bar{n}}^{MC}$: MC Efficiency, $\mathcal{L}_{Int}$: Luminosity

- Theoretically, the Born cross section of the $e^+e^- \to n\bar{n}$ is expressed in this form:

$$\sigma_{Born} = \frac{4\pi\alpha^2\beta}{3q^2}[|G_M|^2 + \frac{2m_n^2}{q^2}|G_E|^2]$$

- The effective form factor is defined as a linear compination of G_E and G_M FFs which is proportional to the square root of the nucleon pair production cross section:

$$|G_{eff}| = (\frac{3q^2}{4\pi\alpha^2\beta(1+\frac{2m_n^2}{q^2})})^{\frac{1}{2}}\sqrt{\sigma_{Born}}$$

Analysis Results

Born Cross Section and Effective Form Factors

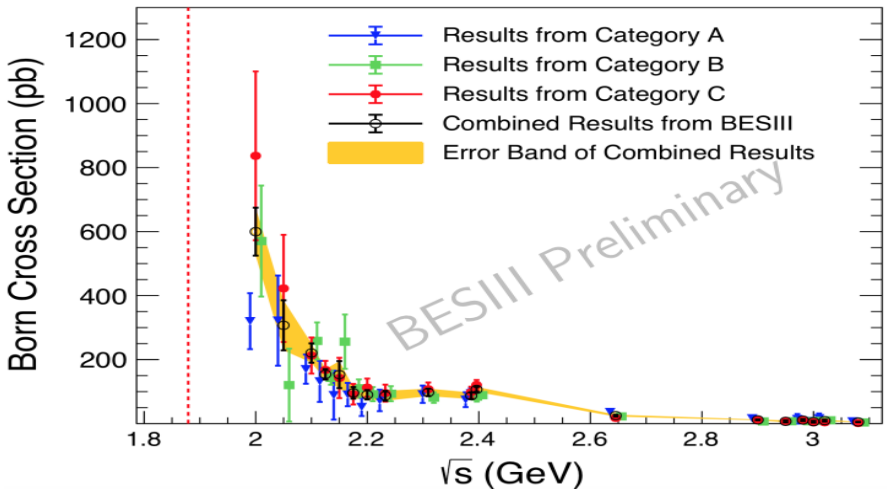

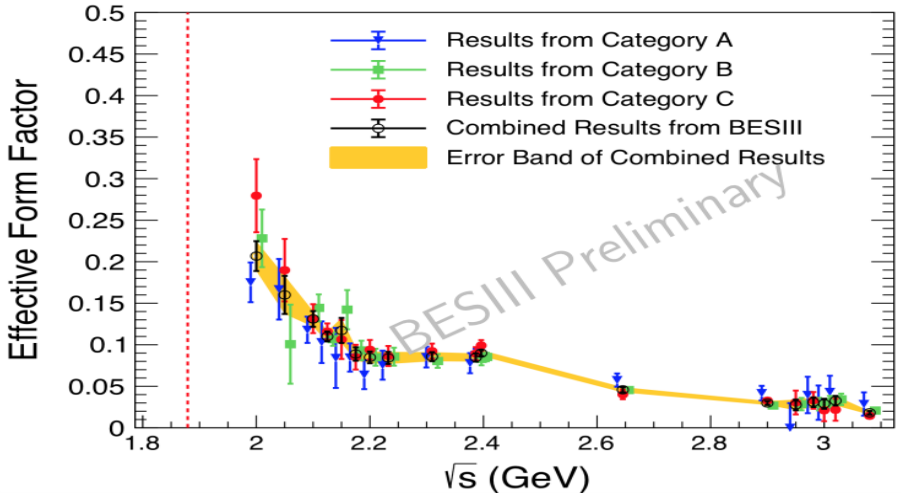

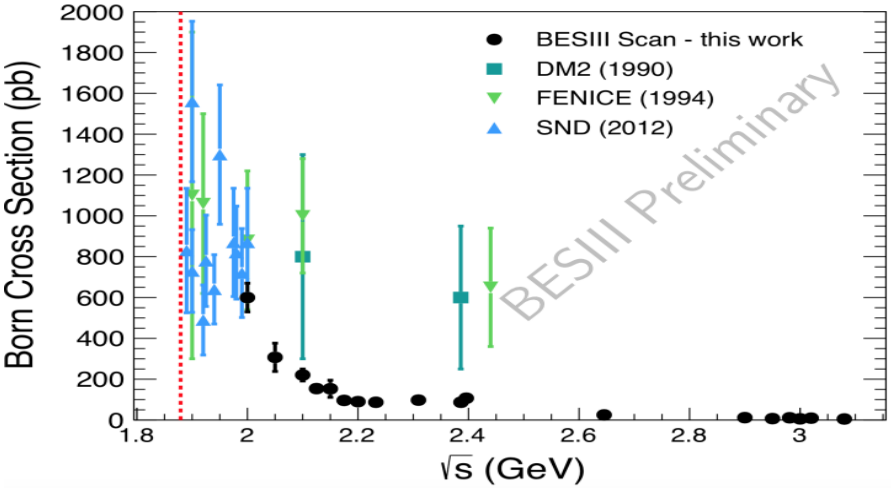

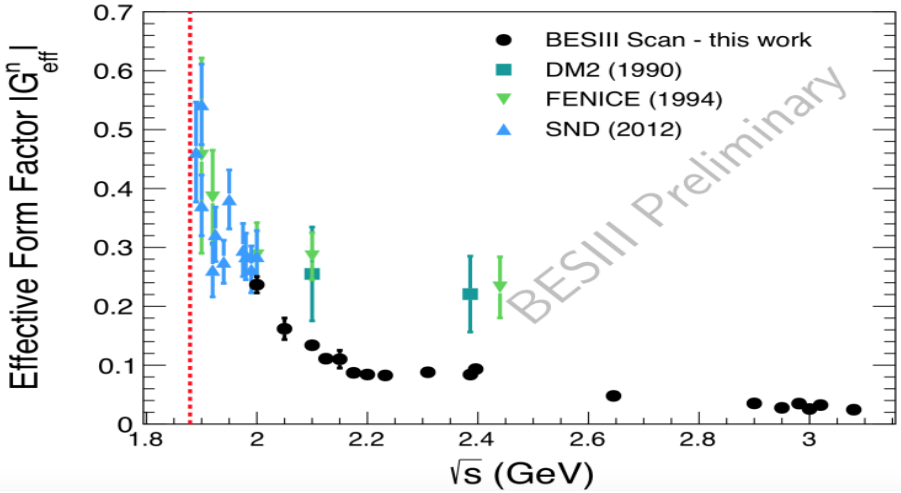

Analysis Results

Oscillation Behavior in the Effective Form Factor

- An oscillation of the effective form factor of proton is observed by BaBar and then confirmed by BESIII.
- **What about the effective form factor of the neutron? Does a similar oscillation exist?**

$$F_p = |G_{eff}^{n,p}(q^2)| - G_D(q^2),\ q^2 = s$$

$$G_D(q^2) = \mathcal{A} \cdot \frac{1}{(1 - \frac{q^2}{0.71(GeV)^2})^2} \cdot \frac{1}{(1 + \frac{q^2}{m_a^2})}$$

- The normalisation $\mathcal{A}$ is extracted by a fit to the effective FF of the neutron:

$$\mathcal{A} = 4.86 \pm 0.09$$

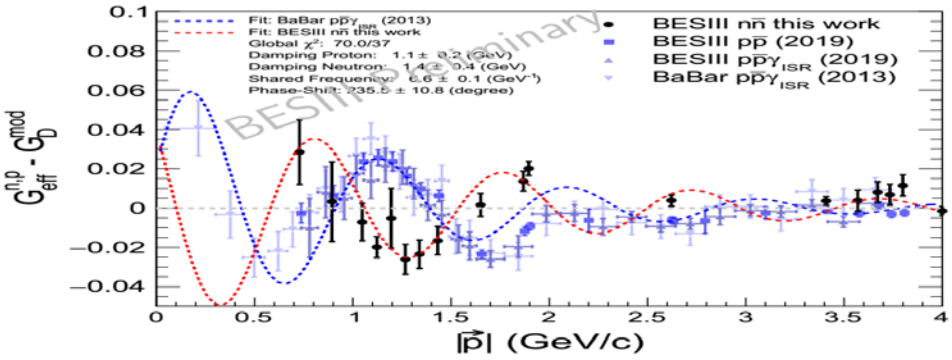

- **An oscillation behavior is observed in the effective form factor of the neutron.**
- **The oscillation is observed with a relative phase shift of ~235° compare to that for the proton.**

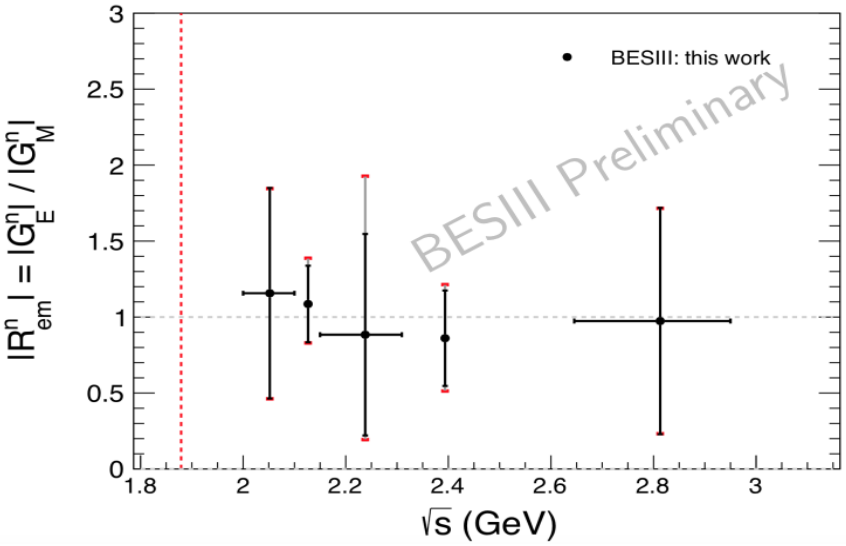

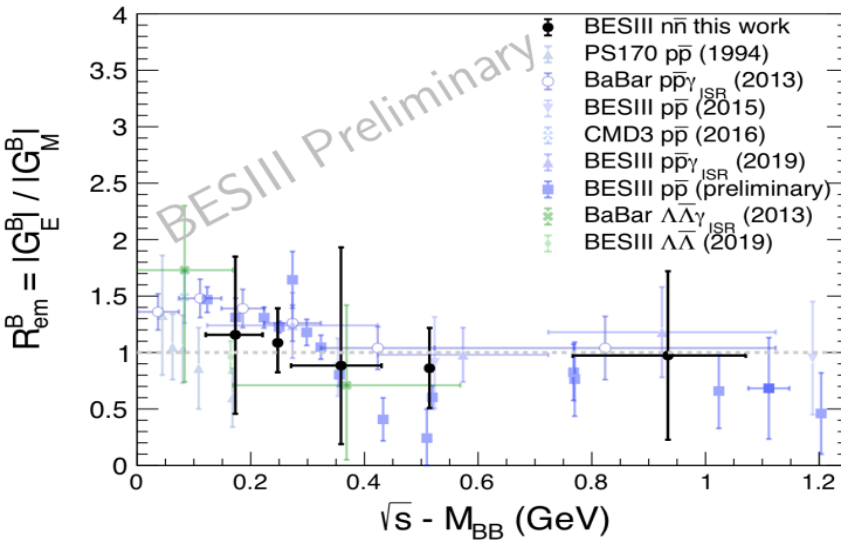

Analysis Results

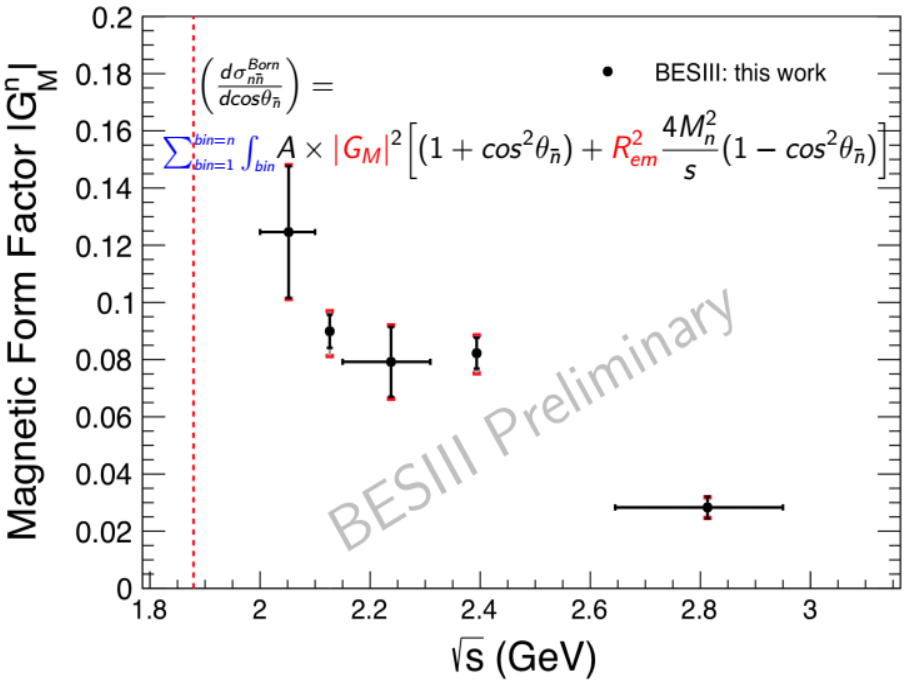

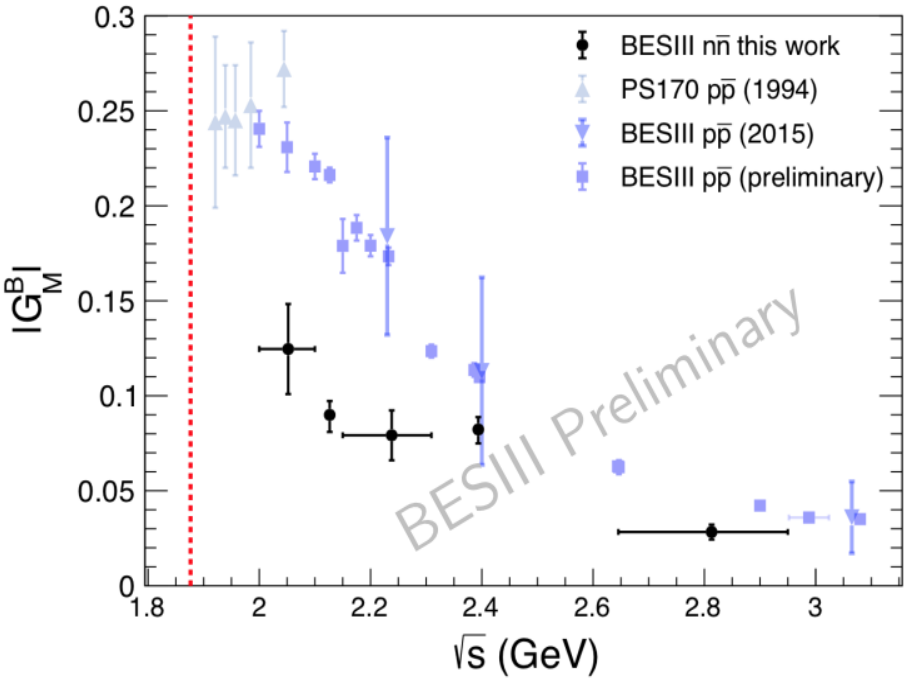

- **The magnetic form factor has been determined for the first time in the TL region at $\sqrt{s}$>2.0 GeV.**
- **The uncertainties of the magnetic form factor results are dominated by the statistical one.**
- **The statistical precision of the $|G^n_M|$ is 9.5% and 7.1% at $\sqrt{s}$= 2.125 and $\sqrt{s}$= 2.394 GeV.**

Cross section measurement of $e^+e^- \to \Lambda\bar{\Lambda}$ with BESIII at 2.3960 GeV

Status on hyperon FFs

Rare experimental results on Hyperon FF

Phys. Rev. D **76,** 092006 (2007)

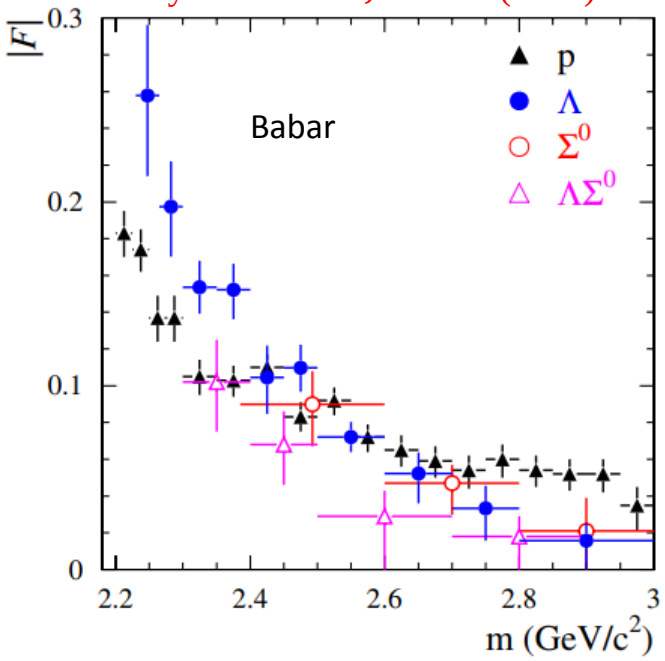

Phys. Lett. B 739 (2014) 90–94

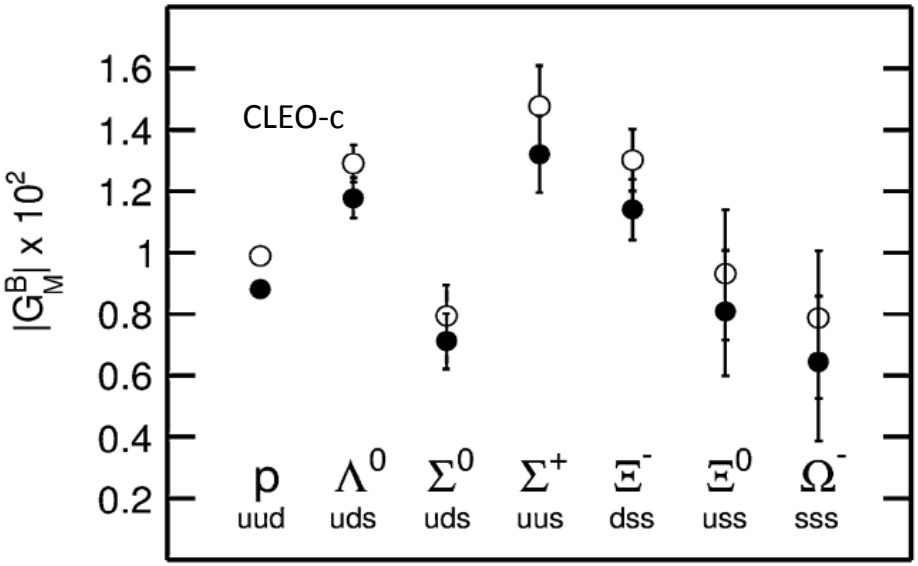

q^2=14.2 GeV^2

- diquark correlation evidence
- favor spin–isospin singlet

Hyperons structure

- Electromagnetic From Factors (EMFFs)
  - fundamental hadron structure observables
  - describe the deviation from the point-like case
  - related to the charge- and magnetization density
- EMFFs of nucleon can be studied in:
  - elastic scattering, $e^- N \to e^- N$, space-like
  - annihilation, $e^+e^- \to N\bar{N}$, $N\bar{N} \to e^+e^-$, time-like
- Hyperons are difficult to study in the space-like region
  - they are unstable – hyperon targets are unfeasible
  - the quality of hyperon beams is in general not sufficient
- e^+e^- annihilation offers the best opportunity to study hyperon structure.

Data sample and event selection

$\sqrt{s}$(GeV)	Run No.	Lumi.(pb^{-1}) offline
2.396	40459-40769	66.869$\pm$0.017$\pm$0.461

- Track level
  - Polar angle: $|cos\theta|$ <0.93
  - Momentum should be less than 0.5 GeV
  - At least 4 tracks
- Tracks with $p < 0.2$GeV are assigned to be $\pi^+\pi^-$
- Tracks with $p > 0.2$ GeV are assigned to be $p\bar{p}$
- Secondary vertex fit to reconstruct Λ and $\bar{\Lambda}$
- Four constraint Kinematic fit to Λ and $\bar{\Lambda}$
  - $\chi^2(4C) < 50$
  - Optimized by the value of figure of merit (FOM) $\frac{S}{\sqrt{S+B}}$
- $|M(p\pi^-/\bar{p}\pi^+) - m_\Lambda|$ <0.006 GeV, m_Λ is the mass of Λ from PDG

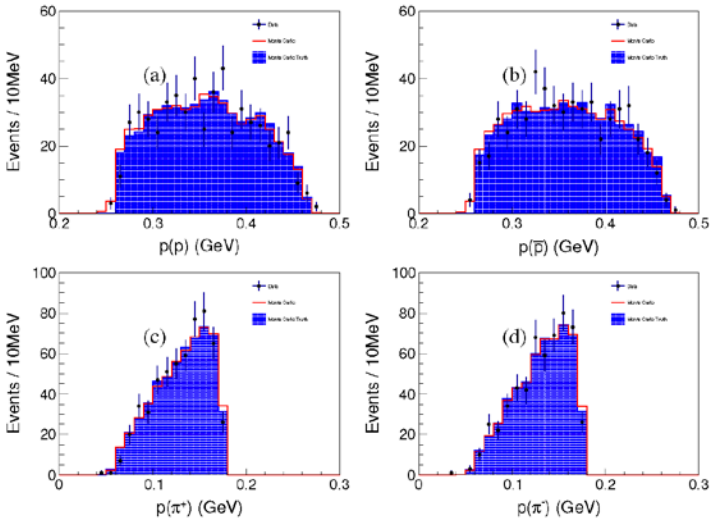

Results of Born cross section and effective EMFFs

- With data collected at $\sqrt{s} = 2.396$ GeV, large statistic
- By exclusive decay mode, i.e. $\Lambda \to p\pi^-, \Lambda \to \bar{p}\pi^+$
- The Born cross section $\sigma_{Born} = \frac{N\_signal}{(L\varepsilon(1+\delta)Br(\Lambda\to p\pi^-)Br(\Lambda\to p\pi^+)}$
  - ISR correction factor 1+δ is from ConExc
  - is the detection efficiency , L is the luminosity
  - σ_{Born}= 118.7 $\pm$5.3(stat)$\pm$ 5.1(syst) pb
- Effective form factor are related to σ_{Born} , |G(q^2)|= $\sqrt{\frac{\sigma_{Born}(q^2)}{(1+\frac{1}{2\tau})(\frac{4\pi\alpha^2\beta}{3q^2})}}$
  - |G|=0.123$\pm$0.003(stat)$\pm$0.003(syst)

$\alpha \approx \frac{1}{137}$ is the fine structure constant, $\beta = \sqrt{1-\frac{1}{\tau}}$ is the velocity , $\tau = \frac{q^2}{4m_\Lambda^2}$

Complete measurement of Λ EMFFs @ $\sqrt{s}$=2.396 GeV

An event of the reaction $e^+e^- \to \Lambda(\to p\pi^-)\bar{\Lambda}(\to \bar{p}\pi^+)$ is specified by the five dimensional vector $\xi = (\theta, \Omega_1, \Omega_2)$, the differential cross section is:

$$\mathcal{W}(\xi) = \mathcal{T}_0(\xi) + \eta\,\mathcal{T}_5(\xi) - \alpha_\Lambda^2\left(\mathcal{T}_1(\xi) + \sqrt{1-\eta^2}\cos(\Delta\Phi)\,\mathcal{T}_2(\xi) + \eta\,\mathcal{T}_6(\xi)\right) + \alpha_\Lambda\sqrt{1-\eta^2}\sin(\Delta\Phi)\left(\mathcal{T}_3(\xi) - \mathcal{T}_4(\xi)\right).$$

Phys. Lett. B 772, 16 (2017)
Phys. Rev. Lett. 123, 122003 (2019)

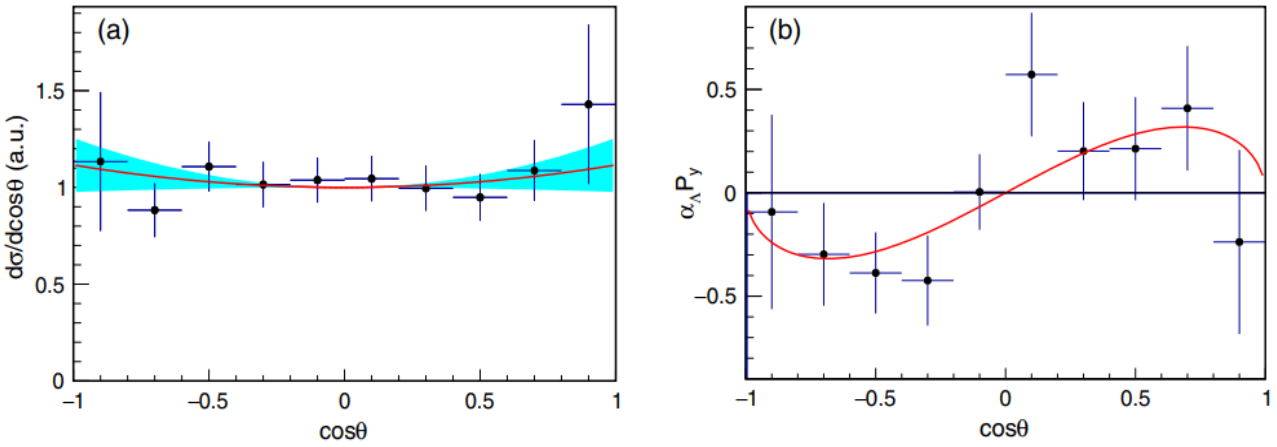

- σ= 118.7±5.3(stat)±5.1(syst) pb
- |G|= 0.123±0.003(stat) ±0.003(syst)
- R=|G_E/G_M|=0.96±0.14(stat) ±0.02(syst)
- $\Delta\Phi = 37^o \pm 12^o(\text{stat}) \pm 6^o(\text{syst})$

Non-zero phase means: not only the s-wave but also the d-wave amplitude contribute to the production
interference between s-d waves results in a polarized final state.
The first complete hyperon EMFF measurement, and a milestone in the study of hyperon structure.

Phys. Rev.Lett 123, 122003 (2019)

Precision measurement of Cross Section Near Threshold with $e^+e^- \to \Lambda_c^+ \bar{\Lambda}_c^-$

Analysis strategy (I)

- Intermediate states are selected in advance.
- Minimum ΔE is required in each mode.
- No optimal requirement at event level.
- Λ_c^+ and $\bar{\Lambda}_c^-$ are reconstructed independently.
- Total cross section is obtained from weighted average.

Data sets

$\sqrt{s}$ (GeV)	$\mathcal{L}_{int}$ (pb^{-1})	Energy error
4.5745	47.67	0.72 MeV
4.580	8.545	–
4.590	8.162	–
4.5995	566.9	0.74 MeV

Decay modes	Absolute BR(%)	Subsequent BR(%)	Total BR(%)
1. $\Lambda_c^+ \to p^+K^-\pi^+$	5.84 ± 0.35	–	5.84 ± 0.35
2. $\Lambda_c^+ \to p^+K_S^0$, $K_S^0 \to \pi^+\pi^-$	1.52 ± 0.09	69.2	1.05 ± 0.06
3. $\Lambda_c^+ \to \Lambda\pi^+$, $\Lambda \to p^+\pi^-$	1.24 ± 0.08	63.9	0.79 ± 0.05
4. $\Lambda_c^+ \to p^+K^-\pi^+\pi^0$, $\pi^0 \to \gamma\gamma$	4.53 ± 0.38	98.8	4.48 ± 0.38
5. $\Lambda_c^+ \to p^+K_S^0\pi^0$, $K_S^0 \to \pi^+\pi^-$, $\pi^0 \to \gamma\gamma$	1.87 ± 0.14	69.2 × 98.8	1.28 ± 0.10
6. $\Lambda_c^+ \to \Lambda\pi^+\pi^0$, $\Lambda \to p^+\pi^-$, $\pi^0 \to \gamma\gamma$	7.01 ± 0.42	63.9 × 98.8	4.43 ± 0.27
7. $\Lambda_c^+ \to p^+K_S^0\pi^+\pi^-$, $K_S^0 \to \pi^+\pi^-$	1.53 ± 0.14	69.2	1.06 ± 0.10
8. $\Lambda_c^+ \to \Lambda\pi^+\pi^+\pi^-$, $\Lambda \to p^+\pi^-$	3.81 ± 0.30	63.9	2.43 ± 0.19
9. $\Lambda_c^+ \to \Sigma^0\pi^+$, $\Sigma^0 \to \Lambda\gamma$, $\Lambda \to p^+\pi^-$	1.27 ± 0.09	63.9	0.81 ± 0.06
10. $\Lambda_c^+ \to \Sigma^+\pi^+\pi^-$, $\Sigma^+ \to p\pi^0$, $\pi^0 \to \gamma\gamma$	4.25 ± 0.31	51.6 × 98.8	2.17 ± 0.16

10 modes branching fraction

Analysis Strategy (II)

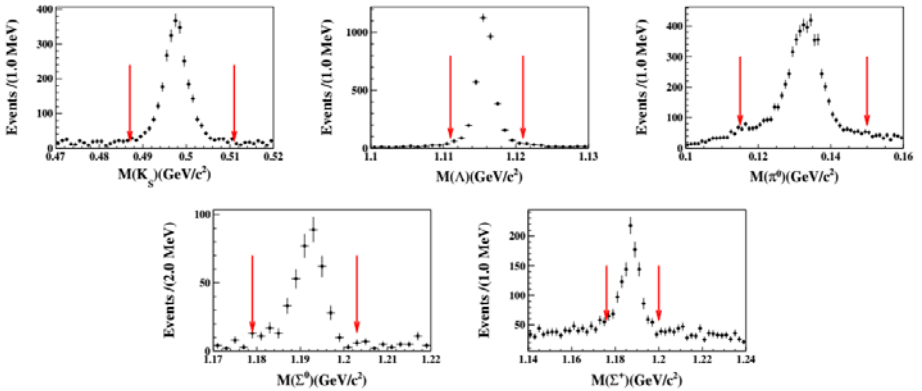

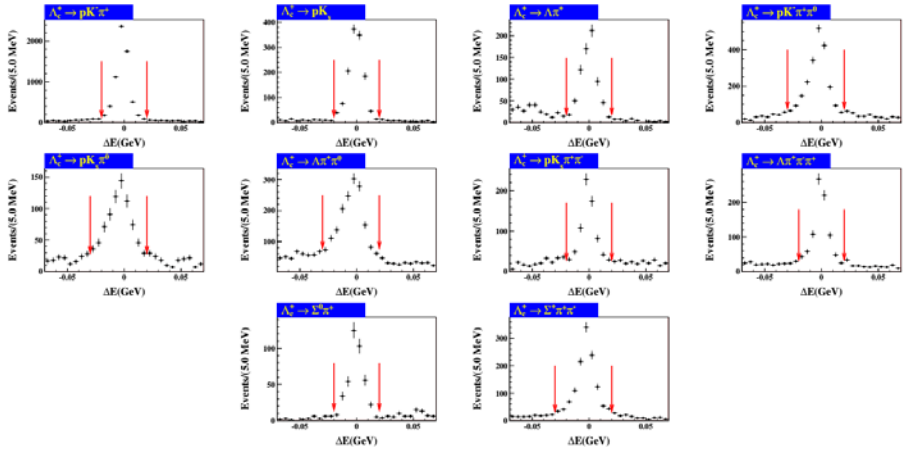

Mode	ΔE window (GeV)
$pK^-\pi^+$	(-0.02,0.02)
pK^0_S	(-0.02,0.02)
$\Lambda\pi^+$	(-0.02,0.02)
$pK^-\pi^+\pi^0$	(-0.03,0.02)
$pK^0_S\pi^0$	(-0.03,0.02)
$\Lambda\pi^+\pi^0$	(-0.03,0.02)
$pK^0_S\pi^+\pi^-$	(-0.02,0.02)
$\Lambda\pi^+\pi^+\pi^-$	(-0.02,0.02)
$\Sigma^0\pi^+$	(-0.02,0.02)
$\Sigma^+\pi^+\pi^-$	(-0.03,0.02)

$$\Delta E = E - E_{\rm beam}$$

$$M_{BC} = \sqrt{E^2_{\rm beam}/c^4 - |\vec{p}|^2/c^2}$$

Background Analysis

signal modes	Background modes										Total Survived
	$pK^-\pi^+$	pK_s^0	$\Lambda\pi^+$	$pK^-\pi^+\pi^0$	$pK_s^0\pi^0$	$\Lambda\pi^+\pi^0$	$pK_s^0\pi^+\pi^-$	$\Lambda\pi^+\pi^+\pi^-$	$\Sigma^0\pi^+$	$\Sigma^+\pi^+\pi^-$	
$pK^-\pi^+$	261769	10	1	145	23	58	4	30	2	143	263074
pK_s^0	21	49980	23	0	3	4	0	0	7	5	50138
$\Lambda\pi^+$	0	5	29995	1	0	2	0	0	83	0	30269
$pK^-\pi^+\pi^0$	1597	3	3	71151	53	114	68	133	2	148	78110
$pK_s^0\pi^0$	210	22	17	132	21157	343	118	43	15	83	23806
$\Lambda\pi^+\pi^0$	34	3	45	6	96	57844	0	260	838	154	63378
$pK_s^0\pi^+\pi^-$	59	2	1	232	145	45	18472	402	4	45	21507
$\Lambda\pi^+\pi^+\pi^-$	3	0	2	14	2	179	33	23176	1	5	24694
$\Sigma^0\pi^+$	0	0	119	0	0	37	0	0	16086	0	16615
$\Sigma^+\pi^+\pi^-$	531	38	3	165	99	322	42	161	19	33334	37015
Total Generated	509030	89999	71591	418112	116115	416653	90768	218187	69165	182799	–

modes		Background modes									
		$pK^-\pi^+$	pK_S^0	$\Lambda\pi^+$	$pK^-\pi^+\pi^0$	$pK_S^0\pi^0$	$\Lambda\pi^+\pi^0$	$pK_S^0\pi^+\pi^-$	$\Lambda\pi^+\pi^+\pi^-$	$\Sigma^0\pi^+$	$\Sigma^+\pi^+\pi^-$
signal modes	1. $pK^-\pi^+$	99.5	0.0	0.0	0.1	0.0	0.0	0.0	0.0	0.0	0.1
	2. pK_S^0	0.0	99.7	0.0	0.0	0.0	0.0	0.0	0.0	0.0	0.0
	3. $\Lambda\pi^+$	0.0	0.0	99.1	0.0	0.0	0.0	0.0	0.0	0.3	0.0
	4. $pK^-\pi^+\pi^0$	2.0	0.0	0.0	91.1	0.1	0.1	0.1	0.2	0.0	0.2
	5. $pK_S^0\pi^0$	0.9	0.1	0.1	0.6	88.9	1.4	0.5	0.2	0.1	0.3
	6. $\Lambda\pi^+\pi^0$	0.1	0.0	0.1	0.0	0.2	91.3	0.0	0.4	1.3	0.2
	7. $pK_S^0\pi^+\pi^-$	0.3	0.0	0.0	1.1	0.7	0.2	85.9	1.9	0.0	0.2
	8. $\Lambda\pi^+\pi^+\pi^-$	0.0	0.0	0.0	0.1	0.0	0.7	0.1	93.9	0.0	0.0
	9. $\Sigma^0\pi^+$	0.0	0.0	0.7	0.0	0.0	0.2	0.0	0.0	96.8	0.0
	10. $\Sigma^+\pi^+\pi^-$	1.4	0.1	0.0	0.4	0.3	0.9	0.1	0.4	0.1	90.1

All cross feed rates are less than 2% and typically are about 1%

Systematic uncertainty

- (Tracking) PID efficiencies are weighted with (transverse) momentum.
- K_S^0 and Λ reconstruction uncertainty with tracking and PID uncertainties of the decay daughter included.
- systematic uncertainty of reconstructing π^0.
- MC statistical uncertainty.
- MC signal modeling uncertainty.
- Uncertainty of subsequent BRs and absolute BRs.

Mode	Tracking	PID	K_S^0	Λ	π^0	MC stat.	Signal model	Sub. BR.	Abs. BR.	Total
1. $pK^-\pi^+$	3.2	4.6	–	–	–	0.3	–	–	6.0	8.2
2. pK_S^0	1.3	0.5	1.2	–	–	0.6	0.2	0.1	5.6	5.9
3. $\Lambda\pi^+$	1.0	1.0	–	2.5	–	0.7	0.5	0.8	6.1	6.9
4. $pK^-\pi^+\pi^0$	3.0	7.6	–	–	1.0	0.8	2.0	–	8.3	11.9
5. $pK_S^0\pi^0$	1.0	1.8	1.2	–	1.0	1.0	1.0	0.1	7.5	8.0
6. $\Lambda\pi^+\pi^0$	1.0	1.0	–	2.5	1.0	0.6	0.6	0.8	5.9	6.8
7. $pK_S^0\pi^+\pi^-$	2.8	5.3	1.2	–	–	1.0	0.5	0.1	9.3	11.2
8. $\Lambda\pi^+\pi^+\pi^-$	3.0	3.0	–	2.5	–	0.8	0.8	0.8	7.9	9.4
9. $\Sigma^0\pi^+$	1.0	1.0	–	2.5	–	1.0	1.7	0.8	6.7	7.6
10. $\Sigma^+\pi^+\pi^-$	3.0	4.0	–	–	1.0	0.7	0.8	0.6	7.4	9.0

Systematic uncertainty

- f_{ISR} uncertainties.
  - Uncertainty of calculation algorithm: **KKMC** and **Kami**.
  - Uncertainty of input line-shape motivated by specific fit model.
  - The uncertainty of CMS energy near threshold: 4574.50 ± 0.72 MeV.
  - Uncertainty of beam energy spread: $\sigma_{beam} = 1.551 \pm 0.175$ MeV.
- Uncertainties of f_{VP}.
- Uncertainties of luminosity.

	$f_{\rm ISR}$						
$\sqrt{s}$ (MeV)	Calculation model	Line shape	C.m. energy	Energy spread	Total	$f_{\rm VP}$	$\mathcal{L}_{\rm int}$
4574.5	3.4	1.2	18.0	3.0	18.6	0.5	1.0
4580.0	0.7	0.6	···	0.2	0.9	0.5	0.7
4590.0	0.2	1.7	···	···	1.7	0.5	0.7
4599.5	0.1	2.6	···	···	2.6	0.5	1.0

Total Born Cross Section

The Born cross section of channel i:

$$x_i = \frac{N_i}{L \cdot \varepsilon_i \cdot f_{VP} \cdot f_{ISR} \cdot BR_i} \tag{1}$$

The total Born cross section:

$$\bar{x} = \sum_i w_i x_i, \; w_i = (1/\sigma_i^2) \Big/ \left(\sum_i 1/\sigma_i^2 \right) \tag{2}$$

and corresponding uncertainty takes the form

$$\sigma_{\bar{x}}^2 = \sum_{i,j} w_i (\mathbf{M}_x)_{ij} w_j \tag{3}$$

or approximately

$$\sigma_{\bar{x},stat.}^2 = \sum_{i,j} w_i (\mathbf{M}_x^{stat.})_{ij} w_j \quad \text{and} \quad \sigma_{\bar{x},syst.}^2 = \sum_{i,j} w_i (\mathbf{M}_x^{syst.})_{ij} w_j \tag{4}$$

The total Born cross sections:

$\sqrt{s}$(GeV)	$\mathcal{L}_{int}$ (pb^{-1})	f_{ISR}	$\sigma^{Born}_{\Lambda_c^+}$ (pb)	$\sigma^{Born}_{\bar{\Lambda}_c^-}$ (pb)	$\overline{\sigma^{Born}}$ (pb)
4.5745	47.67	0.45	$243 \pm 16 \pm 48$	$230 \pm 16 \pm 45$	$236 \pm 11 \pm 46$
4.580	8.545	0.66	$180 \pm 23 \pm 12$	$241 \pm 26 \pm 16$	$207 \pm 17 \pm 13$
4.590	8.126	0.71	$262 \pm 28 \pm 18$	$231 \pm 26 \pm 15$	$245 \pm 19 \pm 16$
4.5995	566.9	0.74	$238 \pm 4 \pm 15$	$236 \pm 4 \pm 15$	$237 \pm 3 \pm 15$

- Efficiencies are obtained by fitting the MBC of signal MC
- A similar fit as that performed on data

Angular distribution study

- Studied at $\sqrt{s} = 4.5745$ and 4.5995 GeV only.
- Divided to 10 *cosθ* bins.
- In each bin, combined signals from all tagged modes.
- Corrected the yields with the detection efficiency bin-by-bin.
- Combined the corrected yields from Λ_c^+ and $\bar{\Lambda}_c^-$ bins.

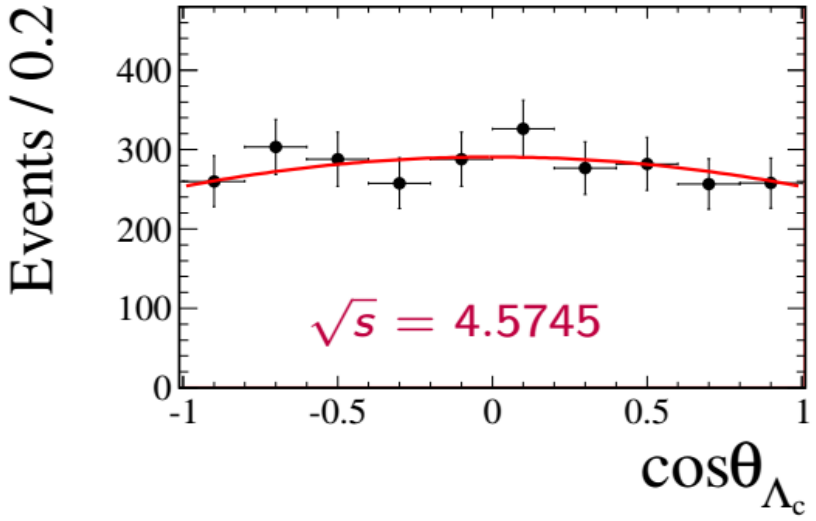

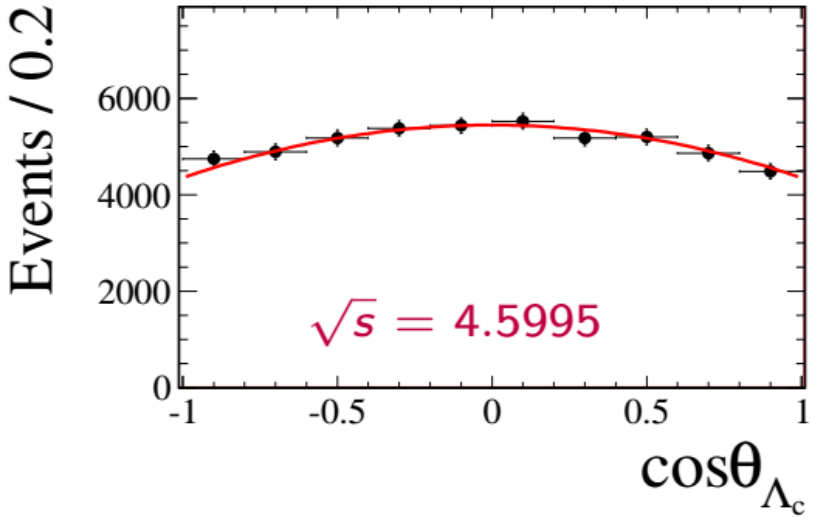

Angular distribution study

The $|G_E/G_M|$ ratios are connected with the α_{Λ_c} by following formula:

$$|G_E/G_M|^2 = (1-\alpha_{\Lambda_c})/(\frac{4m^2_{\Lambda_c^+}}{s}\alpha_{\Lambda_c} + \frac{4m^2_{\Lambda_c^+}}{s})$$

$\sqrt{s}$ (GeV)	α_{Λ_c}	$\lvert G_E/G_M \rvert$
4.5745	$-0.13 \pm 0.12 \pm 0.08$	$1.14 \pm 0.14 \pm 0.07$
4.5995	$-0.20 \pm 0.04 \pm 0.02$	$1.23 \pm 0.05 \pm 0.03$

Analysis Results

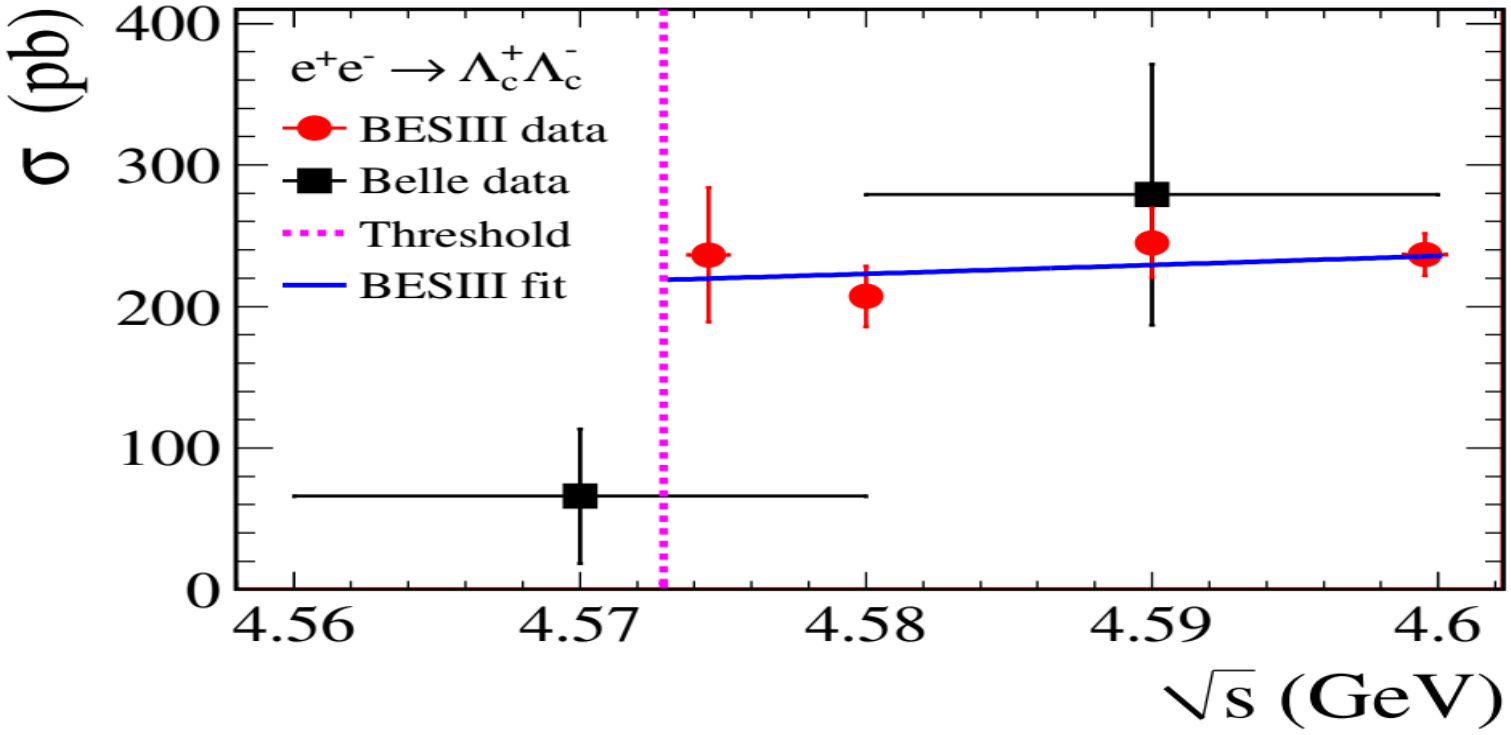

Born cross section of e+e- → $\Lambda_c^+\bar{\Lambda}_c^-$ are measured with high precision

Phys. Rev. Lett 120,132001(2018)

Summary & outlook

- BESIII is an excellent laboratory for the measurement of Farm factor since both ISR and scan method can be performed with a big data sets
- The Born cross sections of e+e-→$p\bar{p}$ have been measured, consistent with BarBar results ,and the corresponding effective FF |G| under the assumption $|G_E|=|G_M|$,The precision has much improvement.
- Measurement of Neutron Electromagnetic Form factors has preliminary results , G_E and G_M have determined for the first time
- Complete Measurement of the Λ Electromagnetic Form Factors has been done.
- Precision Measurement of the $e^+e^- \rightarrow \Lambda_c^+ \bar{\Lambda}_c^-$ Cross Section Near Threshold has been finished.
- With more data sets in the future , more precise results are expected at BESIII

Thanks for your attention!

Energy scan method vs ISR method

Electromagnetic Form Factors in Time-Like Region

Direct Scan Method:

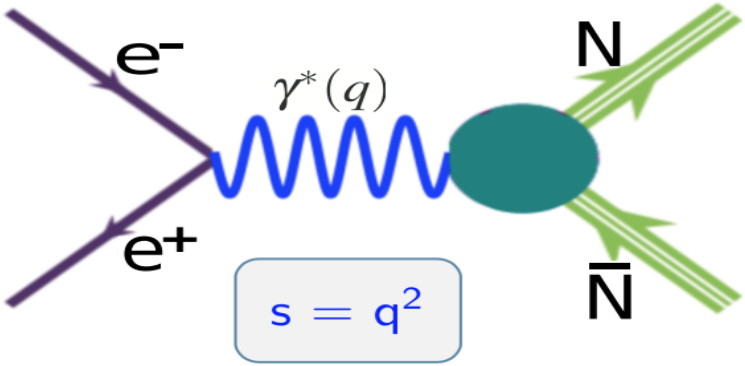

- Beam energy is discrete.
- Luminosity is relatively small.

$$\left(\frac{d\sigma_{N\bar{N}}}{d\Omega}\right) = \frac{\alpha^2 C\beta}{4q^2}\left[|G_M^N|^2(1+cos^2\theta) + \frac{1}{\tau}|G_E^N|^2(1-cos^2\theta)\right]$$

- q^2 is single at each beam energy.

Initial State Radiation Method:

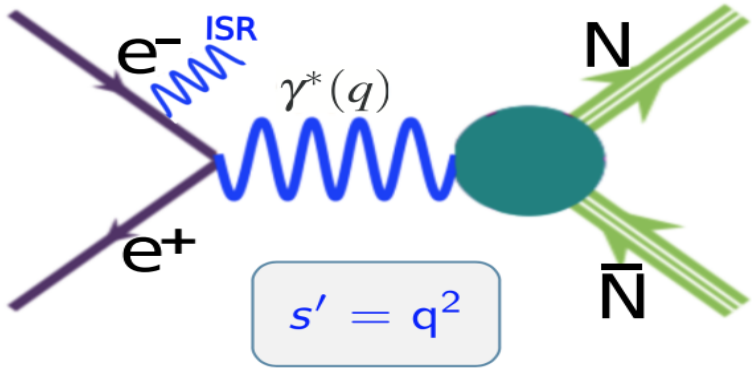

$$s' = x \cong 2E_\gamma/\sqrt{s}$$

- Beam energy is fixed.
- Luminosity is relatively high.

$$\left(\frac{d^2\sigma_{N\bar{N}\gamma}}{dq^2 d\theta}\right) = \frac{1}{q^2} W(q^2, x, \theta_\gamma)\sigma_{N\bar{N}}(q^2)$$

$$W(q^2, x, \theta_\gamma) = \frac{\alpha}{\pi x}\left(\frac{2-2x+x^2}{sin^2\theta_\gamma} - \frac{x^2}{2}\right)$$

- q^2 is continuous from threshold to s.

Time-like vs. space-like EMFFs

- **Space-like region**
  - $e^- B \to e^- B$ scattering
  - $q^2 = (p_{ie} - p_{fe})^2 < 0$
  - G_E and G_M real numbers

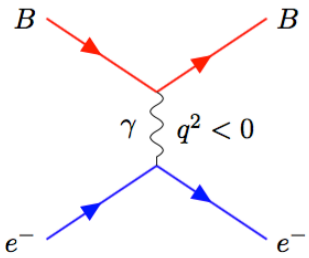

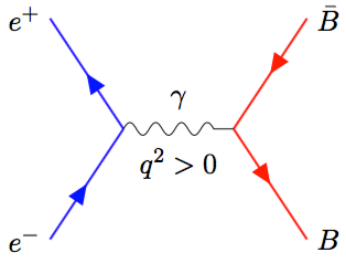

- **Time-like region**
  - $e^+e^- \leftrightarrow B\bar{B}$, $q^2 \geq 4M_B^2 > 0$
  - $G_E(q^2) = |G_E(q^2)|e^{i\Phi_E}$, $G_M(q^2) = |G_M(q^2)|e^{i\Phi_M}$
  - Relative phase: $\Delta\Phi = \Phi_E - \Phi_M$

- **A non-zero phase** has polarization on the final state, even if the initial is unpolarized.